Biosensors and Bioelectronics 175 (2021) 112903

Contents lists available at ScienceDirect

Biosensors and Bioelectronics

journal homepage: http://www.elsevier.com/locate/bios

Induced bioresistance via BNP detection for machine learning-based risk assessment

Seth So [a,*], Aya Khalaf [a], Xinruo Yi [a], Connor Herring [b], Yingze Zhang [c], Marc A. Simon [d], Murat Akcakaya [a], SeungHee Lee [e], Minhee Yun [a,**]

[a] Department of Electrical and Computer Engineering, Swanson School of Engineering, University of Pittsburgh, Pittsburgh, PA, 15261, USA
[b] Department of Chemical Engineering, Swanson School of Engineering, University of Pittsburgh, Pittsburgh, PA, 15261, USA
[c] Departments of Medicine and Human Genetics, University of Pittsburgh, Pittsburgh, PA, 15213, USA
[d] Departments of Medicine (Division of Cardiology), Bioengineering, and Clinical & Translational Science, University of Pittsburgh, Pittsburgh, PA, 15213, USA
[e] Department of Nanoconvergence Engineering and Department of Polymer-Nano Science and Technology, Jeonbuk National University, Jeonju, Jeonbuk, 54896, Republic of Korea

ARTICLE INFO

Keywords:
Biosensor
Machine-learning
Flexible
BNP
Cardiovascular

ABSTRACT

Machine Learning (ML) is a powerful tool for big data analysis that shows substantial potential in the field of healthcare. Individual patient data can be inundative, but its value can be extracted by ML's predictive power and ability to find trends. A great area of interest is early diagnosis and disease management strategies for cardiovascular disease (CVD), the leading cause of death in the world. Treatment is often inhibited by analysis delays, but rapid testing and determination can help improve frequency for real time monitoring. In this research, an ML algorithm was developed in conjunction with a flexible BNP sensor to create a quick diagnostic tool. The sensor was fabricated as an ion-selective field effect transistor (ISFET) in order to be able to quickly gather large amounts of electrical data from a sample. Artifical samples were tested to characterize the sensors using linear sweep voltammetry, and the resulting data was utilized as the initial training set for the ML algorithm, an implementation of quadratic discriminant analysis (QDA) written in MATLAB. Human blood serum samples from 30 University of Pittsburgh Medical Center (UPMC) patients were tested to evaluate the effective sorting power of the algorithm, yielding 95% power in addition to ultra fast data collection and determination.

1. Introduction

Recently there has been rapid progress in the biosensor field. This is due to the adaptation of existing nanofabrication techniques and infrastructure used for modern day electronics to help develop new biosensors with higher precision and more capabilities, including specificity and portability. Additionally, new methods for measuring analytes are being formed using novel materials and technologies like new conducting polymers and electrical sensing methodologies (Kim et al., 2006). Biosensors range in size from microscale to nanoscale and implement many different mechanisms in order to sense and transduce a measurable signal. These include mechanical cantilevers, chemical detection in food and air, and optical identification. Notably, particular advancements have been made into electrical sensing methodologies.

Electrical-based biosensors are able to analyze biomarkers indirectly by measuring different electrical properties. Amperometry takes current time (chronoamperometry) or voltage (voltammetry), and potentiometry measures potential and conductivity changes (Chouteau et al., 2004; Jaffrezic-Renault et al., 2008; Hnaien et al., 2009). Due to this flexibility, electrically operated sensors enjoy the most attention today for their wide array of sensing options. When coupled with small size, nano-scale electronic biosensors offer superior advantages, such as high sensitivity to targets, strong resolution for localized detection, compatibility with standard large-scale semiconductor processing (Qian et al., 2010), and real-time and label-free detection in a nondestructive manner (Luo et al., 2013). Devices with platinum nanoparticles on graphene reduced oxide (Lei et al., 2017) or platinum nanowires (Tong et al., 2010) have been developed to analyze complex matrices like blood. This is some of the most recent progress that uses new nanomaterials in order to demonstrate a novel improvement to electrical

* Corresponding author.1946 Cranbrook Cross, Muscatine, IA, 52761, USA.
** Corresponding author.
E-mail addresses: ses214@pitt.edu (S. So), miy16@pitt.edu (M. Yun).

https://doi.org/10.1016/j.bios.2020.112903
Received 18 March 2020; Received in revised form 25 November 2020; Accepted 13 December 2020
Available online 16 December 2020

biosensing methodology by utilizing the unique chemistry and geometries of nanoparticles to enhance sensing capabilities. Additionally, the new conductive polymer polyaniline has been synthesized as nanowires to sense many analytes in ultra-high resolution on the femtogram regime (Lee et al., 2012), which demonstrates another new nanomaterial being integrated as the primary biosensing element and surpassing the previous resolution limit. Older materials are also being adapted for biosensors - carbon nanotubes have been utilized for their high surface area and functionalization capabilities to reliably detect different molecules at high resolutions (Star et al., 2003; So et al., 2005), which represents a much more general and broad improvement and raises the standards for biosensors as a whole. These three works do an excellent job in characterizing the use of nanomaterials in biosensors by showing strong specificity, high precision, and ability for continuous monitoring. Such advancements have opened the door to substantial improvement in clinical practices With better base characteristics and higher standards for biosensors, new facets of biosensors are being explored that can increase utility, such as use of new data assessment methods for characterization and use of flexible substrates for wearable sensors. This is another advantage that electrical sensors hold over other types. They can be used in dynamic working environment because they depend primarily on conductivity of electrodes, while methods like optical are extremely susceptible to external noise. Standard fabrication techniques can also be used to make biosensors on flexible substrates instead of harder substrates like silicon. In conjunction, these sensors are able to maintain much of the same capabilities of normal sensors but are much more suited to being used in dynamic environments due to their ability to stretch and bend while retaining function.

When fabricated on a flexible substrate, electrical sensors become even more versatile as they have the advantage of being comparatively light while maintaining mechanical strength. Additionally, they can be very thin, which when paired with flexibility, makes flexible substrates very robust and non-brittle. Economically, polymers and plastics are much more affordable but can also have a wide range of physical capabilities. Flexible substrates' potential to be useful in low-cost, dynamic environments make them standout options for a myriad of niche applications such as shear-normal hybrid stress sensors (Hwang et al., 2007), conductive skins for tactile robotics applications, and even liquid filled membranes for microfluidic-based sensing. Flexibles have an especially strong future in medical context for both in-situ and in-vivo applications. Recently, transparent polymers like polyethylene terephthalate (PET) have been growing in use for biosensors as a substrate for patterning electrodes and growing cells for biosensors. These devices allow for a real time monitoring, can provide instant feedback, and have predictive warning capabilities. They offer strong resolution and reliability for their price along with accessibility in daily life. A unique aspect of wearable biosensors is that they are most often noninvasive, gathering different solutions from less commonly analyzed but ubiquitous bioliquids like sweat and saliva (Melzer et al., 2014; Rim et al., 2016). Aside from physical benefits, wearables can often have mental effects as well. Having easily accessible information can help an individual make more informed lifestyle choices and serve as steadfast reminders throughout the day, encouraging user engagement (Ha et al., 2018). Many different types of wearable sensors have been developed for a wide array of purposes. Some take the form of patches, and most recent commercial options involve wrist watches. Other nontraditional forms of wearables are being explored, such as contact lens glucose sensors and tattoo-like perspiration monitors. Regardless of form, wearable sensors have been successfully developed for many purposes ranging from blood glucose (Kudo et al., 2006) for glycemia monitoring to perspiration (Gao et al., 2016) for metabolic analysis and have demonstrated feasibility in many of use cases including cardiovascular context. Wearable sensors for heart disease are gaining traction because they allow for more regular monitoring of heart disease, which is usually diagnosed too late after a major event such as myocardial infarction or the development of heart failure (HF). Applying the diagnostic capabilities of wearable sensors to an area like heart disease presents many exciting opportunities to improve current testing methods.

Cardiovascular disease (CVD) is the leading cause of death in the world and prevalence is increasing, particularly for heart failure (Virani et al., 2020). HF has an incredibly high prevalence and incidence, afflicting ~26 million adults per year globally. Mortality rates remain high but rapid detection and close monitoring would be beneficial to improve outcomes. B-type natriuretic peptide (BNP) is a protein released by the heart when the ventricles undergo strain in order to decrease blood pressure, and it has been found to be an excellent biomarker for CVDs that can be monitored (Kara et al., 2016; Wolsk et al., 2017). However, expensive testing assays, specialized equipment, and intermediary infrastructure can be limiting factors. The development of mass producible, wearable sensors can help abate these problems by enabling regular testing of BNP. Live-monitoring sensors have the ability to decrease overall risk of chronic cardiovascular as well as warn of impending acute myocardial infarction by detecting large changes in BNP concentration (Nalbantić et al., 2012; Suprun et al., 2012; Grabowska et al., 2018). Whereas results from normal testing may take several hours or more to receive, BNP monitored by a wearable sensor can provide instantaneous feedback in a noninvasive manner. Though there can be significant noise in a single test, multiple readings can be taken at once and filter with high power statistical analysis to denoise data and improve accuracy of determination.

Today, there are many different options for data processing, such as analysis of variance (ANOVA) which determines difference between groups due to inter-relational variance, and mechanistic analysis which breaks data sets into input-output relationships. However, these are all causal analyses that only help to explain data. One of the major challenges in current biosensor research is the reproducible data. While most researches have demonstrated excellent sensing performance, there is a general lack of data stability and reproducibility due to large variability in individual devices. Regular monitoring for early diagnosing requires the incorporation of a method like Machine Learning, which has strong causal power as well as a strong predictive power, in order to improve data stability, testing repeatability, and results classification accuracy. Machine Learning (ML) is a type of artificial intelligence which can be used to increase confidence of results. It is a type of statistical modelling that can learn without explicit instructions by using an adaptive classification algorithm to sort sample readings and can be much more accurate than traditional methods. Currently ML is being implemented in many different fields and research due to its high analytic capability – it has proven to be especially useful in image classification, navigation, and big data visualization. Due to its predictive power and diagnostic capabilities, ML may also play a key role in the biosensors scene, because biosensor results are analyzed over long periods of time. Lab results only give insight into one specific instant in the patient's life, but biosensors are powerful because they can monitor and analyze samples much more often and quickly. ML is necessary in order to take advantage of this time frame to identify both current status as well as future trends in the patient's health (Ouchi et al., 2018), greatly increasing predictive power. Previous work has been done to implement ML algorithms into biosensors, including a wrist sensor for seizure detection (Poh et al., 2012) and glucose-oxidase sensor for predictive monitoring (Gonzalez-Navarro et al., 2016). For cardiovascular biosensors, BNP concentration in the blood can translate directly to an individual's risk of developing HF. Using ML to find patterns in daily readings can allow for predictions of future health status, especially in cardiovascular context (Green et al., 2018; Rong et al., 2018). This greatly increases a biosensor's use for early diagnostics and helps realize the concept of lab-on-a-chip (LOC).

In this research, a biosensor was developed using modern nanofabrication techniques to allow for higher specificity, portability, and reproducibility. PET, a low-cost and flexible polymer material, was used as the substrate so that the sensors were light and robust for dynamic environments like being worn by a patient. In order to help with diagnosis of HF, the biosensor was modified for the detection of BNP using

monoclonal antibodies on a PANI growth template. Finally, a machine learning classification algorithm was developed to classify the immunoassay-based patient readings into two categories, healthy or at-risk. This system is the prototype for making a lab-on-a-chip wearable sensor to allow for regular BNP testing. Important design considerations for creating a viable on-site diagnosis option included size, reproducibility, and cost. Devices were fabricated and characterized in collaboration with the Signal Processing and Statistical Learning Group and the Cardiovascular Institute of the University of Pittsburgh Medical Center.

2. Material and methods

2.1. Chemicals and reagents for substrate preparation and modification

Acetone, IPA, DI water, N_2 gas, LOR-b, SC1827, Chromium, Gold, 351 and AZK developer were all used from clean room facility's stock. Aniline [$C_6H_5NH_2$], Ammonium persulfate [$(NH_4)_2\ S_2O_8$], Perchloric acid [$HCLO_4$], EDC [$C_8H_{17}N_3$], NHS [$C_4H_5NO_3$], and bovine serum albumin (BSA) were purchased from Sigma Aldrich. Mouse anti-BNP and recombinant Human BNP were purchased from Novus Biologicals. All dilutions were made with 0.01× PBS.

2.2. Device fabrication

A sheet of PET was cut into the shape of 4" wafer and cleaned with acetone for 5 min followed by a bath in isopropyl alcohol for 3 min to remove the acetone. Excess isopropyl alcohol was evaporated with inert nitrogen gas. This cleaning process and all subsequent work took place in a clean room fume hood to decrease risk of contamination. After cleaning, the PET wafer was wet mounted to a silicon wafer by pipetting several drops of DI (deionized) water onto the silicon wafer before gently putting the PET wafer on top. The wet mount provided enough adhesion and a rigid body that would enable the PET wafer to be spin-coated with Laurell spinners. First, a layer of LOR-b (lift off resist-b), a photoresist optimized for metal ion developers, was spin coated on at 3000 rpm for 45 s, then baked at 115 °C for 2 min. After the first minute, a preheated silicon wafer was placed directly on top of the PET wafer to complete baking. Second, photoresist SC1827, a positive resist optimized for g-line exposure, was spin-coated on at 4500 rpm for 45 s to adjust for viscosity. The PET was hard baked following the same baking procedure, but the preheated silicon wafer was held steady to hover above the PET wafer without making contact to avoid any undesired sticking between the two.

The MLA100 from Heidelberg Instruments, a liquid crystal maskless laser aligner, was used to expose an electrode pattern designed in AutoCAD, at a dose of 240 mW/cm^2, found in previous dosage tests. The wafer was then developed in a 1:4 solution of AZK400, a developer complimentary to the LOR-b resist used earlier. The wafer was observed under an infrared microscope to check for proper exposure. Next, 80 nm of gold and 5 nm of platinum were deposited on via electron deposition by a Plassys machine. Gold was chosen for its high conductivity and resistance to oxidation, and the small amount a platinum was added to increase elasticity without greatly affecting conductivity. Lift off was performed with 1165 remover to dissolve the remaining resist and any metal not directly deposited onto the PET wafer due to the bilayer photoresist. With the electrodes deposited, the wafer was ready for PANI growth to bridge the electrodes.

2.3. PANI growth

The same lithography process was used to create an exposed area bridging the electrodes onto which polyaniline (PANI) was chemically synthesized. PANI is an intrinsically conductive organic polymer that is known for its low ionization potential and high electron affinity. PANI was used here as a p-type semiconductor that was capable of entrapping other biological molecules. The PET wafer with gold-platinum electrodes was submerged in a beaker of 200 mL deionized water (set in an ice bath to maintain a consistent low temperature environment). The water was protonated with 6 mL of perchloric to control the pH of the solution and avoid unwanted products. 911 μg of aniline was slowly mixed in, followed by 700 mg of aqueous ammonium per sulfate (APS), which acted as the oxidant. The solution was mixed by stir bar at 300 rpm to encourage polymerization of aniline monomers nucleated onto the surface of the wafer for 90 min before the reaction was halted. After growth, any PANI not chemically adhered to the exposed electrodes or PET was washed off in an acetone bath for 5 min before being rinsed with water.

2.4. Surface modification

Because PANI and BNP-monoclonal antibodies (mAb) cannot directly bind, surface modification was achieved by using 1-ethyl-3-(3-dimethylaminoprppyl) carbodiimide (EDC) as a crosslinker to bind PANI on one terminal and the antibodies on the other terminal. N-Hydroxysuccinimide (NHS) was added to accelerate the crosslinking process. A uniform solution of antibody, EDC, and NHS was prepared in a 2:49:49 ratio, and the 2.5 μL of this solution was pipetted onto each device and left to adhere to the PANI for 12 h. Another 2.5 μL of 20 $^{ng}/_{mL}$ reconstituted lyophilized bovine serum albumin (BSA) powder was pipetted onto each device 30 min prior to testing in order to prevent non-specific binding during testing.

The resulting device is shown in Fig. 1. The primary substrate is a sheet of PET that is translucent and able to flex. On top are conductive gold electrodes deposited with a small amount of platinum for added structural support. A thin sheet of PANI bridges the two electrodes and serves as the binding site for the mAb. A droplet of serum is then deposited onto the device, and any sample BNP binds to the receptor side of the mAb, inducing a change in gate voltage.

2.5. Electrical measurement

Fig. 2A is an image showing the measurement and characterization set up for the biosensors fabricated in this research. The biosensors are on clear, flexible substrate, sitting on a controllable stage. Devices were vacuum mounted onto on a 3 axis stage (x, y, Θ). Fig. 2B is a close-up showing how the probe contacts the device during testing. The 2 μL droplets of control serum can be seen on the PANI sheet bridging the electrodes, like Fig. 1. After surface modification and BSA blocking, a motorized 6 channel copper probe was lowered onto the gold contacts for electrical connection, and optimized gate voltage of −0.4 V was applied with an external power source from Rigol Technologies. Devices were then tested with linear sweep voltammetry using a potentiostat from CH Instruments. The sweep was run from [0–0.4] V, measurements

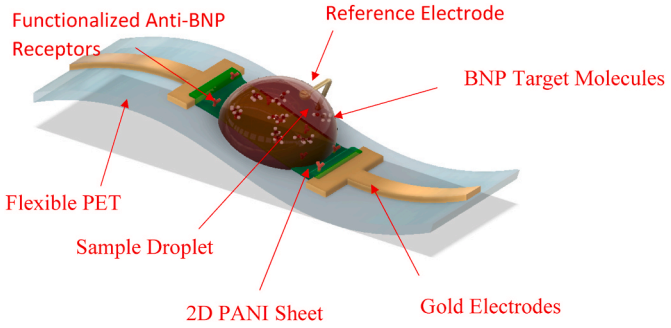

Fig. 1. CAD rendering of ISFET biosensor, labelled with red are: PET substrate, PANI sheet bridge, gold-chromium electrodes, reference electrode, functionalized antibodies, blood sample, and BNP molecules. Each PET wafer holds a 5 × 5 array of cells, each containing 6 devices (150 ISFETs total). Cell size is 1 cm by 1 cm. (For interpretation of the references to color in this figure legend, the reader is referred to the Web version of this article.)

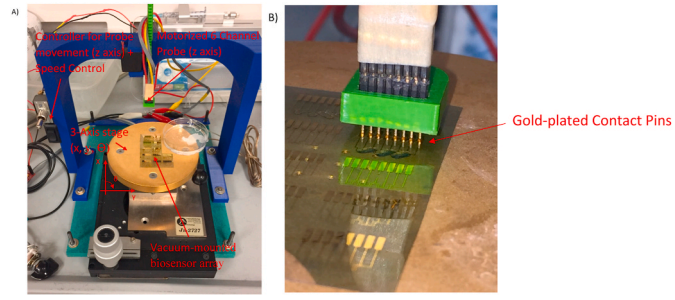

Fig. 2. View of overall (A) measurement set up, annotated with: probe mechanism, moving stage, motor driver, vacuum mount. Additionally, an up close view (B) of 6 channel probes lowered onto gold contacts. The left most is the reference electrode contact, the middle 6 are the counter electrodes for 6 individual sensor devices, and the right most contact is for the universal working electrode. Probes are made from copper. (For interpretation of the references to color in this figure legend, the reader is referred to the Web version of this article.)

were taken every 5 ms, and sensitivity was set to nanoampere scale. The current response and reference charge were locally recorded using the same instrument.

2.6. Machine learning algorithm and PCA

A single layer neural network was coded in python to separate sample trials into 2 categories, healthy or unhealthy. Healthy samples served as the control, while unhealthy was defined according to the outside edge of the gray area, that is any concentration [C] > 1000 pg/mL, and unhealthy is labelled as anything below. The neural network first used linear discriminant analysis (LDA) to classify samples. LDA is a statistical method key for preprocessing data for pattern-classification by reducing degrees of freedom. Doing so helps avoid overfitting, which happens when the ML algorithm incorporates noise deterministically into the model. With 30 training samples for each, healthy and unhealthy, the dependent variable of a rough formula for BNP concentration was made in terms of the statistical mean and variation of the electrical measurements – that is to say that BNP concentration was expressed as two linear combinations of other independent features. Within and between class scatter matrices, S_W and S_B respectively, were calculated according to standard Fisher LDA algorithms to characterize the variance of the training data. Features were then extracted from the resultant covariance matrix though eigen decomposition and separated according to minimal error function by minimization of S_W and maximization of S_B:

$$\boldsymbol{S_W} = \boldsymbol{\Sigma}_{classes}\left[\boldsymbol{\Sigma}_{class}(\boldsymbol{A}_{class} - \boldsymbol{\mu}_{class})(\boldsymbol{A}_{class} - \boldsymbol{\mu}_{class})^T\right]$$

$$\boldsymbol{S_B} = \boldsymbol{\Sigma}_{class}(\boldsymbol{\mu}_{class} - \boldsymbol{\mu})(\boldsymbol{\mu}_{class} - \boldsymbol{\mu})^T$$

$$\boldsymbol{\Sigma}_{WB} = \boldsymbol{S}_W^{-1}\boldsymbol{S}_B \text{ , (pseudoinverse)}$$

When electrical measurements were taken from new samples, the data set's statistical output was input into the ML predictive model to predict which group the data came from. Test data was sorted to whichever linear combination had a stronger correlation, hence classifying a sample test as either healthy or unhealthy. In order to extend the capability of the ML algorithm and create more robust results, a second assessment method was conducted through quadratic discriminant analysis. QDA is a more robust variation of LDA. It assumes that the covariance matrices are not identical between each variable. This is accomplished by computing quadratic terms in addition to linear terms, leading to a more thorough set of measurement vectors before determining linear combinations to fit the data into. Doing so gives one extra degree of freedom for the model and with it higher statistical power. A secondary analysis of the results was performed using principal component analysis (PCA) for a reference to compare results using similar methods. Methods followed are widely available in existing literature (Richman, 1986; Sneyers et al., 1989; Jollife, 1990; Stewart et al., 2014). The code was programmed in MATLAB 2015b for both feature extraction of the IV curves and PCA analysis. No constraints were applied and only the first 3 components were taken. All samples were plotted against 3 three statistical properties of the sample readings themselves. As results were confirmed or corrected, the sorted data was added to the ML algorithm so that it could become more robust for future predictions.

2.7. Human samples

Deidentified samples from healthy controls and patients with CVD were obtained from an ongoing heart failure registry at the University of Pittsburgh. The protocol was approved by the Institutional Review Board. All subjects provided informed consent and chose to remain fully anonymous. Venous blood was collected using Vacutainer serum tube, Blood samples were kept at room temperature for 30 min and centrifuged at 1500×*g* for 15 min in a table-top centrifuge. Doing so separated larger molecules from the sample such as hemoglobin and platelets to reduce contaminant noise and increase signal to noise ratio. Serum samples were collected and stored in multiple aliquots at −80 C. Prior to testing with biosensors, each aliquot was tested and labelled for BNP concentration using validated commercial ELISA kits. When transferred for biosensor testing, individual aliquots were warmed in ambient to room temperature before being pipetted manually onto the sensors. Each aliquot was then immediately returned to the freezer, and freeze-thaw cycles were given special attention.

3. Results and discussion

3.1. Sensitivity

8 artificially graded concentrations of BNP in healthy human serum were tested on the devices to explore the range of device response. Serum was derived from human plasma by spin separating the hemoglobin with a centrifuge at 2000 rpm for 2 min, and then separated into 7 aliquots of differing BNP concentration. Trace amounts of hemoglobin have negligible effects on conductivity (Hirsch et al., 1950; Zhbanov et al., 2015) Up to 0.25 V, the current response was linear, as shown in

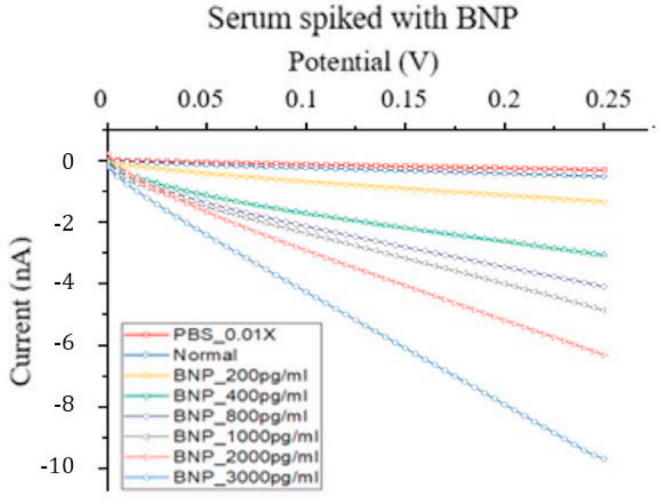

Fig. 3. Current response results from spike testing experiment for PBS, control sample, 200, 400, 800, 1000, 2000, and 3000 $^{pg}/_{mL}$. Linearly increasing current responses demonstrate proper function of the biosensor. Gate voltage is −0.4 V due to p-type nature of PANI and prior testing.

Fig. 3, at which point separation began to become more significant. This serves as confirmation of the well-known fact that increased BNP concentration corresponds directly with greater total accumulation of protein charge, creating a higher gate voltage (Kim et al., 2006). By this point, all samples had differentiated according to their respective concentrations in near logarithmic spacing. This demonstrated that the devices were able to successfully respond to samples according to their concentration and served as validation that the biosensors could support the required range of BNP containing the low/high threshold concentration.

Samples with higher BNP concentrations were able to bond more fully with the anti-BNP adhered onto the PANI bridge. Doing so creates a buildup of negative charge onto functionalized the PANI substrate, which induces a slight positive alteration to the gate voltage, hence allowing more current to flow through the device. This experiment was conducted to confirm the average concentration of BNP in serum derived from a healthy patient's blood. It had a slightly higher response that non-conductive 0.01X PBS, as there was little BNP contained in the sample. However, when spiked with increasingly higher concentrations of BNP, the current response increased immediately, confirming that the bonded BNP was altering the gate voltage to allow a greater current response. Broadly, this result gives strong indication that the biosensor framework can be expanded for further antigen-detection based risk assessment with the modification of different antibodies.

3.2. Baseline testing

As relatively little research has been conducted using human blood or serum, 10 aliquots of serum were drawn from each of 10 healthy subjects and tested to provide a reference current response and check for device testing repeatability. These aliquots were tested across 10 devices and superimposed onto a single graph to show a visual average current response. The current responses develop a heat map with the dark regions showing denser sampling responses shown in Fig. 4A. From the graph, the average current at 0.4 $V_{gate} = 0.3$ nA and a total range of 1 nA. Each voltage sweep resulted in a linear current response, which suggests that a chemical stability between PANI-receptors and BNP has been achieved. Across the 80 total tests, variance was less than 1 nA, with even tighter ranges within each device, shown in Fig. 4B. The max variance of measurements in each device was 0.8 nA, and the variance across all samples was 0.93 nA. These results suggest good repeatability within and across each device. These results were consistent with expectations and showed that the devices were compatible with human serum samples. As expected, the healthy samples yielded a current response on the pico-amp regime, with some outliers breaching 1 nA by the end of the voltage sweep.

3.3. A.I. Classification

The machine learning algorithm was tested by providing a set of 42 targets and 42 non targets after 2 generations of training. The samples came in 5 different concentrations of BNP defined in this study: healthy 1 (control 1), healthy 2 (control 2), 600 pg/mL, 800 pg/mL, and 1800 pg/mL. Primary testing divided the samples into two groups: not at-risk (healthy 1, heathy 2, and 600 pg/mL) and at-risk (800 pg/mL and 1800 pg/mL). Fig. 5 below shows the input readings color coded according to concentration. Visually, the samples started to differentiate similarly to the spike test from Fig. 1. Strong separation was achieved, clearly distinguishing each sample by 0.4 V. Variance between samples increased with higher concentrations as expected and resulted in overlap between several samples, especially with 800 pg/mL trials. This labelled characteristic was suited to be a primary feature for PCA. Additionally, the current magnitude seems to saturate with increased BNP, a characteristic that could be modulated with an increase of anti-BNP concentration during surface modification. In all cases, healthy samples displayed minimal response.

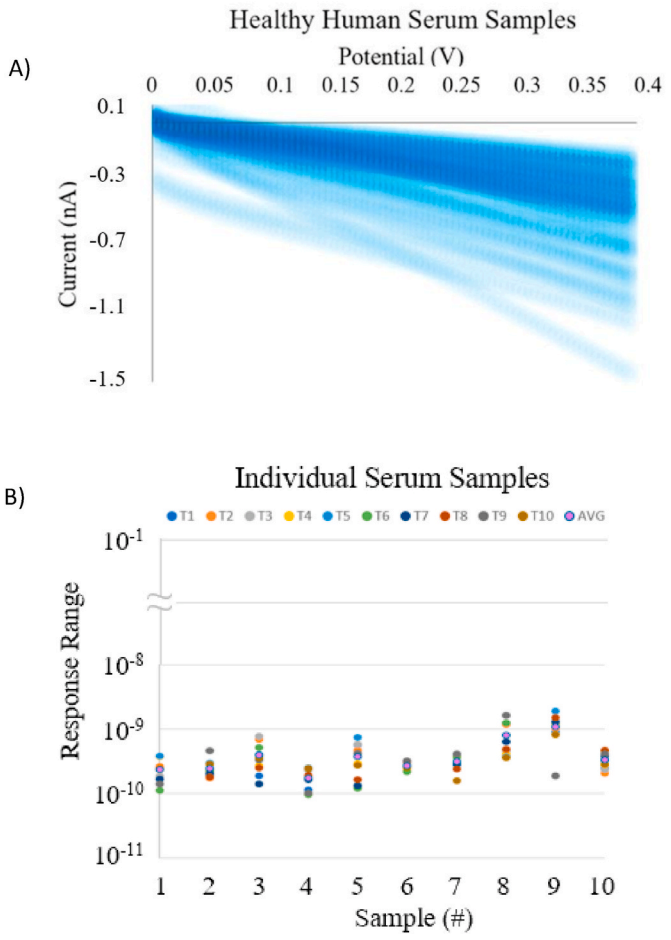

Fig. 4. Current responses for 100 baseline (healthy patient blood samples) tests across 10 samples. Each test has 80 points taken during a linear sweep from 0 to 0.4 V (A) Results are plotted to form a heatmap – darker regions indicated higher density of results among multiple samples and lighter regions indicate more sparse measurements and variance plot (B) organized according to devices that each measurement was taken from. Results characterize range of current response according to a healthy level of BNP.

Fig. 6 shows these results in a confusion matrix. Reading the matrix horizontally first tells the rate of actual success – the first row displays that 41 out of 42 unhealthy samples were correctly predicted and the second row shows that 39 out of 42 controls were correctly identified. Reading vertically analyzes the statistical power of the model – the first column tells the α (type 1) error and the second column gives β (type 2) error. Green highlighted squares indicate desired results, while red indicates misclassifications. After the second generation, the algorithm was able to achieve an overall accuracy of 95%, precision of 93%, and a recall of 98%. Therefore, the current algorithm with the given sample set has an F-score of 0.95 indicating high power.

The PCA results are displayed in Fig. 7. The components were mean of the current response, variance of the current response, and mean of the reference charge respectively. As a result, there are two clear groups of clustering with small overlap. The blue grouping were points all classified as the control healthy serum samples, and the orange points were classified as high BNP concentration samples. The analysis was able to identify 28/30 targets 99/100 non targets correctly, which also gives an F-score of 0.95, indicating similar power. Therefore, the ML algorithm is comparable in statistical power to PCA, which is a benchmark for separation classifiers. Another possible advantage of PCA is the low computing and power requirements, simplicity of calculation, and little set up required. The results are suitable for a rapid diagnosis system, whereas a higher power algorithm may exceed the needs of such a

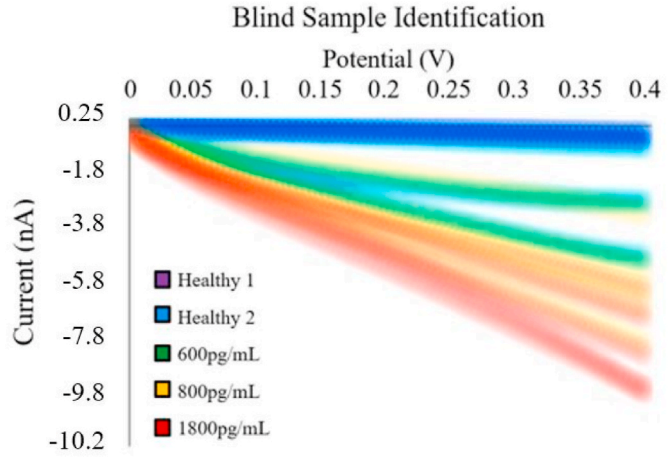

Fig. 5. Blind test current responses were color coded according to concentration (control 1, control 2, 600, 800, and 1800 pg/mL and confusion matrix. Results show clear separation between healthy patients and those with high levels of BNP in blood. As BNP concentration was increased, variance increased significantly at higher gate voltage. Clear separation was achieved between blood samples with trace amounts of BNP and patients with at-risk levels of BNP. (For interpretation of the references to color in this figure legend, the reader is referred to the Web version of this article.)

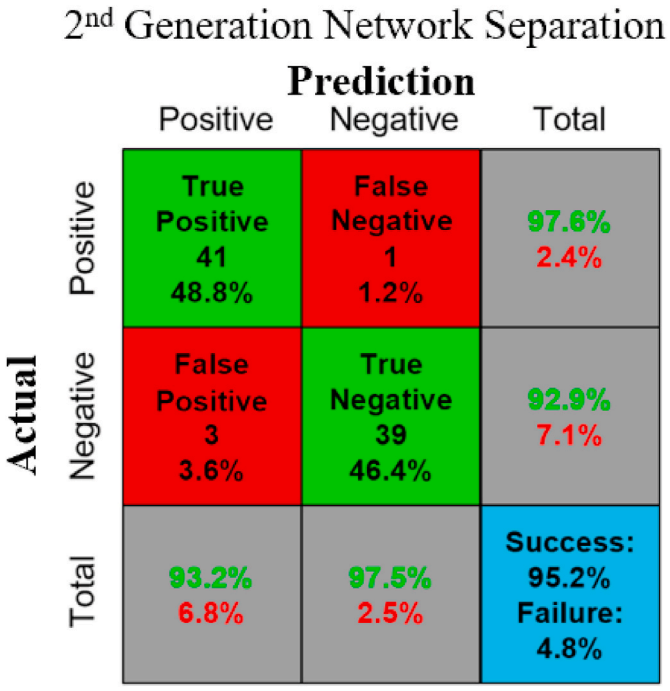

Fig. 6. Confusion matrix of classifier results were used to calculate power, alpha and beta error, and prevalence. All results were comparable to golden standard methods such as PCA

device. However, simpler networks, such as the single layer implemented here, are demonstrated for feasibility and efficacy.

4. Conclusions

This research has demonstrated the fabrication and characterization of a new flexible PANI-based biosensor able to sense BNP on pg/mL and ng/mL regime for lab-on-a-chip applications. The sensor is immunoassay based functions via voltammetry, making it both highly selective and nondestructive. Results suggest compatibility with human serum

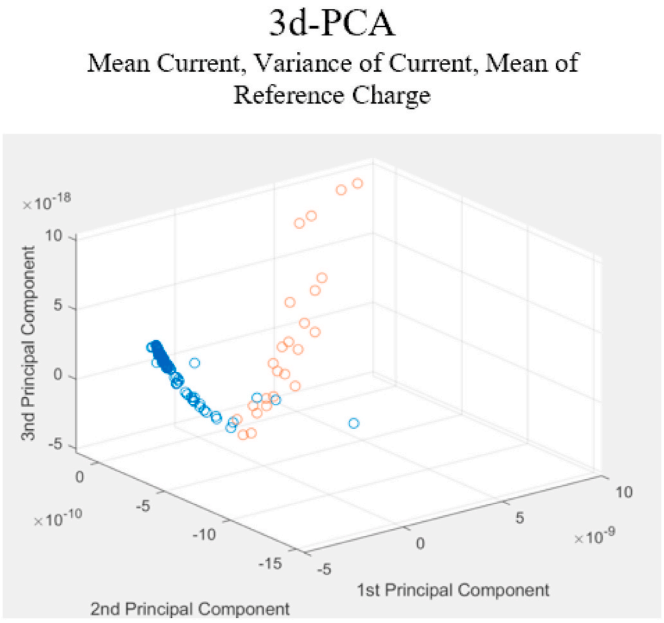

Fig. 7. Independent 3 d-PCA analysis of blind test samples. Components were mean current, current variance, and mean charge. Blue indicates samples classified as healthy and Orange indicates samples classified as unhealthy. 2 clusters were found according to training – healthy and unhealthy. Performance was slightly better than ML algorithm due to small amount of training data. (For interpretation of the references to color in this figure legend, the reader is referred to the Web version of this article.)

derived from blood, so protein competition is yet to be tested. Spike testing exhibited functionality and signal characterization; baseline testing showed biocompatibility with real human serum samples. Most importantly, results from blind testing demonstrate a ML algorithm comparable in power to a 3-dimensional PCA, achieving 95% power. This statistical method was able to be used for label prediction and enhance stability of data, indicating strong potential use in diagnostic applications, thereby showing feasibility of the new data assessment method.

CRediT authorship contribution statement

Seth So: Overall experiment, Writing original draft. **Aya Khalaf:** Machine learning experiment. **Xinruo Yi:** Biosensor test and experiment. **Connor Herring:** Biosensor development. **Yingze Zhang:** Blood sample analysis and verification. **Marc A. Simon:** Blood sample design and comments. **Murat Akcakaya:** Machine learning experiment and data analysis. **SeungHee Lee:** Biosensor design and concept development. **Minhee Yun:** Supervision, and design of the biosensor.

Declaration of competing interest

The authors declare that they have no known competing financial interests or personal relationships that could have appeared to influence the work reported in this paper.

Acknowledgements

The authors are grateful for financial support from the National Science Foundation (NSF) CBET 1706620.

References

Chouteau, C., Dzyadevych, S., Chovelon, J.M., et al., 2004. Biosens. Bioelectron. 19 (9), 1089–1096.

Durak-Nalbantic, A., Dzubur, A., Dilic, Mirza, 2012. Bosn. J. Basic Med. Sci. 12 (3), 164–168.
Gao, W., Emaminejad, S., Nyein, et al., 2016. Nature 529, 509–514.
Gonzalez-Navarro, F.F., Stilianova-Stoytcheva, M., Renteria-Gutierrez, L., et al., 2016. Sensors 16 (11), 1483.
Grabowska, I., Sharma, N., Vasilescu, A., et al., 2018. Am. Chem. Soc. 3 (9), 12010–12018.
Green, E., Mourik, R., Wolfus, et al., 2018. Circulation 136 (1).
Ha, M., Lim, S., Ko, H., 2018. Royal Society of Chemistry 6, 4043–4064.
Hirsch, F., Texter, E., Wood, L., et al., 1950. Am. Soc. Hematol. 5 (11), 1017–1035.
Hnaien, M., Hassen, W., Abdelghani, A., et al., 2009. Electrochem. Commun. 11 (1), 165–168.
Hwang, E., Seo, J., Kim, Y., 2007. J. Micromelectromech. Syst. 6 (3), 556–563.
Jaffrezic-Renault, N., Dzyadevych, S., 2008. Sensors 8 (4), 2569–2588.
Jollife, I.T., 1990. Weather 45, 375–382.
Kara, K., Lehmann, N., Neumann, T., Kalsch, H., et al., 2015. Int. J. Cardiol. 183 (15), 155–161.
Kim, D., Park, J., Shin, J., et al., 2006. Sensor. Actuator. 117 (2), 488–494.
Kudo, H., Sawada, T., Kazawa, E., et al., 2006. Biosens. Bioelectron. 22 (4), 558–562.
Lee, I., Luo, X., Huang, J., et al., 2012. Biosensors 2, 205–220.
Lei, Y., Xiao, M., Li, Y., et al., 2017. Biosens. Bioelectron. 91, 1–7.
Luo, X., Davis, J., 2013. Royal Society of Chemistry 42, 5944–5962.
Melzer, M., Monch, J., Makarov, D., et al., 2014. Adv. Mater. 27 (7), 1274–1280.
Ouchi, K., Lindvall, C., Chai, P., et al., 2018. J. Med. Toxicol. 14 (3), 248–252.
Poh, M.Z., Loddenkemper, T., Reinsberger, et al., 2012. Epilepsia 53 (5), 93–97.
Qian, T., Wang, Y., 2010. Med. Biol. Eng. Comput. 48 (10), 1023–1032.
Richman, M.B., 1986. Rotation of principal components. J. Climatol. 6, 293–335.
Rim, Y., Bae, S.H., Chen, H., et al., 2016. Adv. Mater. 28 (22), 4415–4440.
Rong, Y., Padron, A., Hagerty, K., et al., 2018. Royal Society of Chemistry 143, 2066–2075.
Sneyers, R., Vandiepenbeeck, M., Vanlierde, R., 1989. Theor. Appl. Climatol. 39 (4), 199–204.
So, H., Won, K., Kim, Y.H., et al., 2005. Am. Chem. Soc. 127 (34), 11906–11907.
Star, A., Han, T., Gabriel, J.C., et al., 2003. Am. Chem. Soc. 3 (10), 1421–1423.
Stewart, S., Ivy, M., Anslyn, E., 2014. Royal Society of Chemistry 43, 70–84.
Suprun, E., Saveliev, A., Evtugyn, G., et al., 2012. Bioelectr. Biosensors 33 (1), 158–164.
Tong, D., Tran, P., Pham, X., 2010. Adv. Nat. Sci. Nanosci. Nanotechnol. 1 (1).
Virani, S., Tsao, C., Alonso, A., et al., 2020. Circulation 141 (9).
Wolsk, E., Claggett, B., Pfeffer, M., et al., 2017. J. Am. Heart Assoc. 6 (6).
Zhbanov, A., Yang, S., 2015. PloS One 10 (6).